Composites Part B 78 (2015) 86–94

Contents lists available at ScienceDirect

Composites Part B

journal homepage: www.elsevier.com/locate/compositesb

Comparison and analysis of Acoustography with other NDE techniques for foreign object inclusion detection in graphite epoxy composites

Anish Poudel [a, *], Shashi Shekhar Shrestha [a], Jaswinder Singh Sandhu [b, 1], Tsuchin Philip Chu [a], Charles George Pergantis [c, 2]

[a] Department of Mechanical Engineering and Energy Processes, Southern Illinois University, 1230 Lincoln Drive, Mail Code 6603, Carbondale, IL 62901, USA
[b] Santec Systems, Inc., 2924 Malmo Drive, Arlington Heights, IL 60005-4726, USA
[c] U.S. Army Research Laboratory, Aberdeen Proving Ground, MD 21005-5069, USA

ARTICLE INFO

Article history:
Received 24 November 2014
Received in revised form
13 March 2015
Accepted 15 March 2015
Available online 1 April 2015

Keywords:
A. Carbon fibre
A. Laminates
B. Defects
D. Non-destructive evaluation

ABSTRACT

This paper presents the use of a novel through-transmission ultrasonic (TTU) Acoustography non-destructive evaluation (NDE) method to detect foreign object inclusion (FOI) defects in graphite epoxy composite laminates. The study employed three different composite test standards with varied size FOI defects embedded at varying depth within the composite laminates. For validation, Acoustography results were directly compared with conventional immersion TTU testing and infrared thermography (IRT) methods. From results obtained, it was demonstrated that the Signal-to-Noise Ratio (SNR) measurements for Acoustography were more than 6:1 and were in good correlation with immersion TTU and IRT results. The defect sizing ability of TTU Acoustography for FOI defects in graphite epoxy composite laminates were also in strong correlation with immersion TTU and IRT techniques. Finally, for the three laboratory systems employed in this study, typical panel TTU Acoustography inspection time was just about three minutes to scan a 300 mm × 300 mm (11.8″ × 11.8″) area, which was more than three times faster compared to IRT and sixty times faster to conventional immersion TTU C-Scan techniques. This is a very significant finding for the reason that Acoustography is being developed as a faster, more efficient, and affordable alternative to traditional ultrasonic inspection systems for composite manufacturing quality control and quality assurance (QC/QA) and field maintenance of composite structure applications.

1. Introduction

Advanced Polymer-matrix composites (PMCs) such as graphite epoxy composites, also referred to as carbon fiber reinforced plastics (CFRP), are increasingly being used in many structural applications ranging from aerospace to aircrafts, automotive, industrial, sports industry, and many other consumer products. The main reason for this is, unlike traditional metals and their alloys, composites offer outstanding thermal and physical properties including high strength and stiffness to weight ratios, low coefficient of thermal expansion, high fatigue resistance, inherent corrosion resistance, and low electromagnetic reflectance [1–5]. However, composites are prone to defect mechanisms which can occur either during the processing stages or during in-service operations or in a repair environment. In addition, due to the heterogeneous nature of composites, the form of defects is often very different from those typically found in traditional metals and their alloys, and the fracture mechanisms are also much more complex [6]. Some of the common manufacturing defects that can occur during the production process of composites include micro-cracks, fiber breakage, voids, delamination, porosity, and foreign object inclusions (FOIs). FOIs usually occur mainly due to small foreign debris that can accidentally get included in parent material during manufacture or repair. Common examples of foreign debris are pre-preg backing paper or release film, which is inadvertently left between plies during layup, and tool components such as knife blades. Moreover, FOIs can occur in many different forms and existing NDE techniques are often encountered with difficulties in detecting and characterizing FOIs when they have similar acoustic impedance compared to the composite parts. FOIs can have a degrading effect on

* Corresponding author. Tel.: +1 (618) 453 7049; fax: +1 (618) 453 7658.
E-mail addresses: anish@siu.edu (A. Poudel), j-sandhu@santecsystems.com (J.S. Sandhu), charles.g.pergantis.civ@mail.mil (C.G. Pergantis).
[1] Tel.: +1 (847) 215 8884.
[2] Tel.: +1 (410) 306 0688.

http://dx.doi.org/10.1016/j.compositesb.2015.03.048
1359-8368/

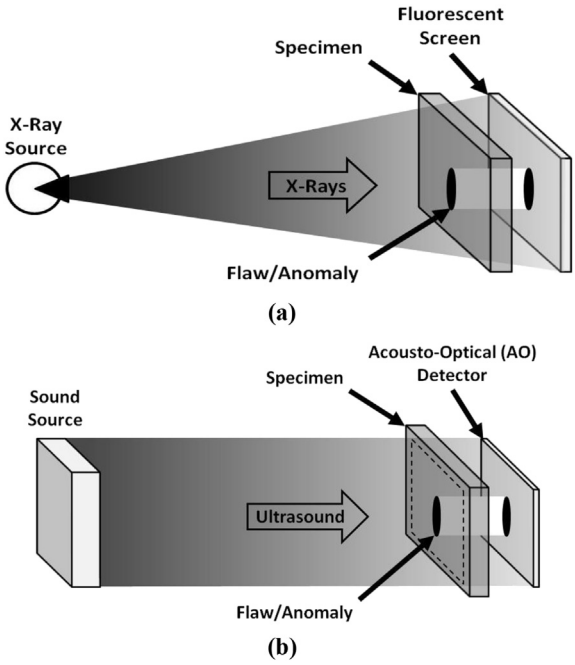

Fig. 1. Comparison of the whole field imaging technology (a) Acoustography; (b) X-ray.

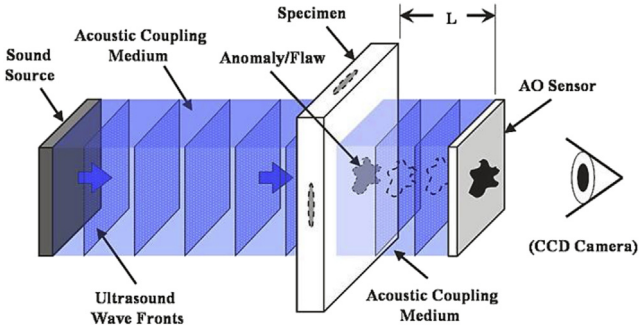

Fig. 2. Working Principle of TTU Acoustography.

mechanical properties and may act as sites of stress concentration (stress raisers) and potential initiation sites for more serious defects such as delaminations and disbonds in composites. This may produce disastrous effects if not identified and corrected within a timely manner. In severe cases, FOIs within aviation/aerospace structures can directly threaten safety of flight crews and integrity of the aircraft/aerospace platform.

Multiple state-of-the art non-destructive evaluation (NDE) techniques are often employed today to detect and characterize flaws and damages in composite structures during manufacturing, in-service, and repair environment. NDE techniques that are commonly applied for foreign object inclusion (FOI) defect detection and characterization can be grouped into broad categories of tap testing [7], ultrasonics [8–13], infrared thermography [2,14–19], laser shearography [20], radiography [21–24], and microwave [25]. All of these techniques have their own advantages and limitation. However, through-transmission ultrasonic (TTU) C-scan, followed by ultrasonic pulse echo A-scan inspections are the primary NDE techniques utilized by industry as quality assurance (QA) checks for the production of composite parts and structures. These inspection techniques require tedious point-by-point inspection of parts that can be time-consuming. Acoustography NDE provides an alternative to point-by-point scanning and offers new capabilities to the NDE engineer. It could be a simple, fast, and economical alternative to conventional ultrasonic testing (UT) methods for the inspection and evaluation of certain composite components and structures [26–29].

In this study, a novel TTU Acoustography technique was applied to detect FOI defects in composite laminate test specimens. The results obtained from this method were compared directly with conventional immersion TTU and Infrared Thermography (IRT) methods. Quantitative comparisons were made to assess correlations between the three methods to assess by measuring the defect Signal-to-Noise Ratio (SNR), defect size, and inspection times.

2. Acoustography principle

Acoustography is a broad-area, nearly real-time ultrasonic imaging technique that provides an alternative to point-by-point UT [30–33]. In this approach, a novel, wide-area acousto-optic (AO) sensor is employed to provide whole-field ultrasonic images analogous to real time x-ray imaging, as shown in Fig. 1.

TTU Acoustography employs an AO-sensor (detector) made from a proprietary mesophase liquid crystal (LC) material. In the TTU Acoustography set-up, the front-side of the AO-Sensor is exposed to an acoustic field and the backside of the AO-Sensor is viewed by an observer or charged couple device (CCD) camera while exposed to polarized light. As ultrasonic beams propagate from the sound source towards the AO-Sensor, any flaws, voids or inclusions that it encounters will produce a differential attenuation. As the beam propagates past the flaw/anomaly region, it casts an ultrasonic "shadow" along its path which is instantly converted into a visual image by the acoustic-optic (AO) sensor located underneath and in near-real time as shown in Fig. 2.

The physical principle by which the AO-sensor converts ultrasonic waves into visual images is based on the birefringent properties of LC materials contained in the sensor [28]. The LC layer exhibits no birefringence in the absence of ultrasound and exhibits a uniform dark field under cross-polarizer viewing. But, when an ultrasonic beam is exposed on the AO-sensor, the LC layer becomes

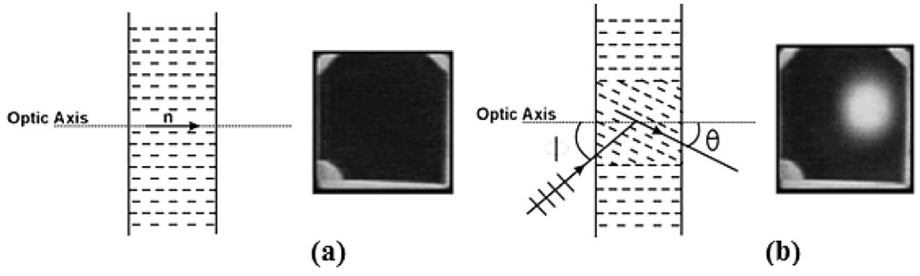

Fig. 3. Effect of ultrasound exposure on AO-sensor. (a) Without ultrasonic exposure; and, (b) With ultrasonic exposure.

birefringent, showing the brightness change (optical density change) under cross-polarizer viewing as shown in Fig. 3. The brightness change can be related to the ultrasonic intensity by AO-sensor acousto-optic transfer curve [33].

3. Experimental setup

This section describes and illustrates the composite test panels that were fabricated for this research work. In addition, the laboratory test set-up of the Acoustography system, as well as the conventional immersion TTU C-scan and IRT test set-ups is also described.

3.1. Sample description

Three graphite epoxy composite test panels were fabricated with engineered FOI defects. FOI defects were made of thin Teflon film having a thickness 0.1 mm (0.004″). Panel A and panel B were fiber-reinforced 16-ply graphite epoxy composite laminates, having a 0.2 mm (0.008″) thickness per ply, with a symmetric orientation

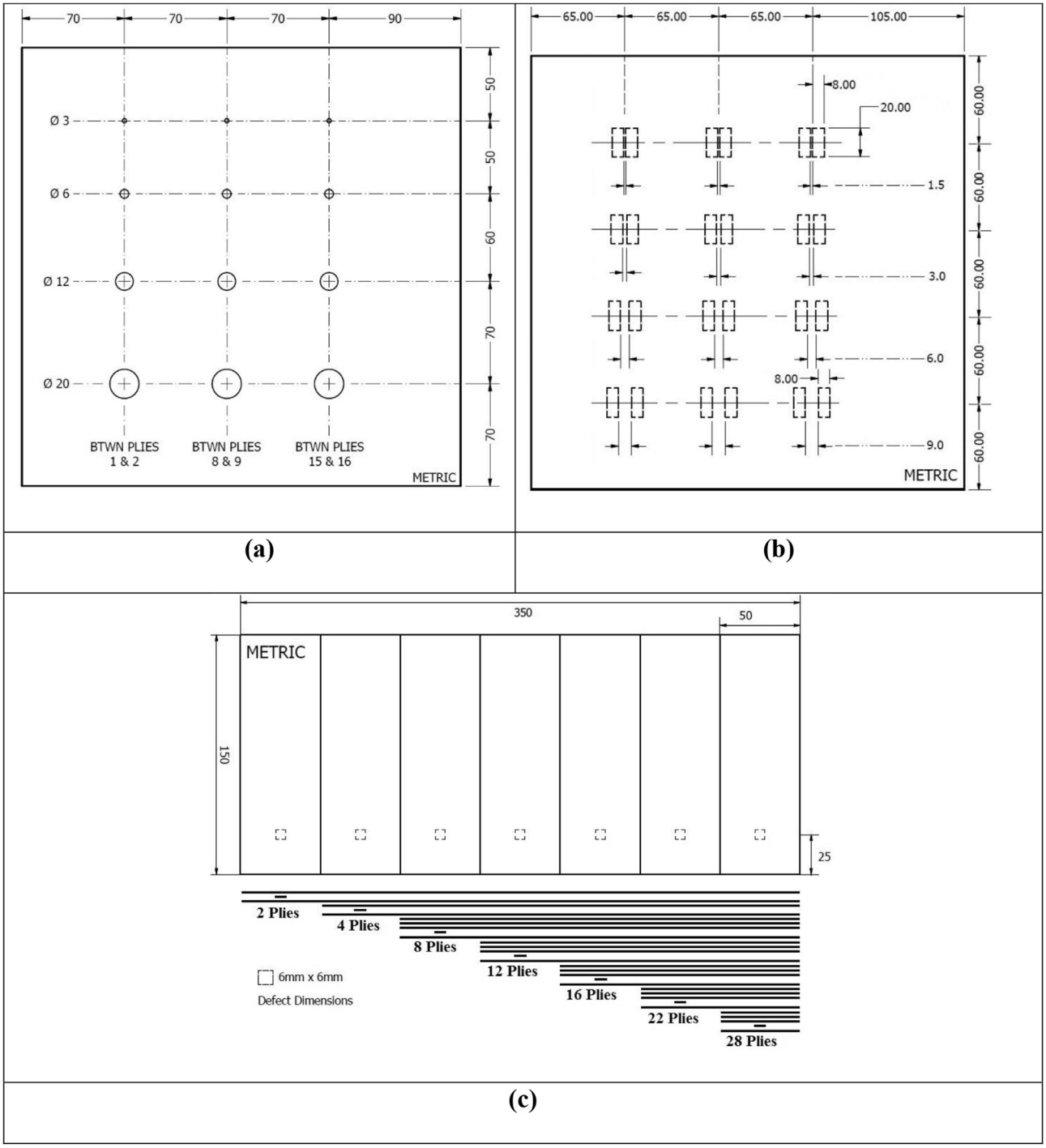

Fig. 4. Engineered defect map in CFRP panels. (a) Panel A; (b) Panel B; and, (c) Panel C.

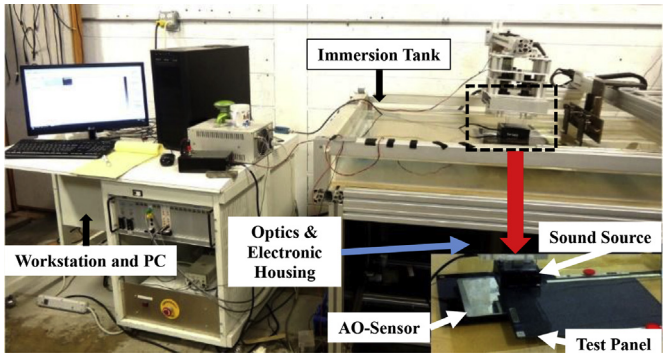

Fig. 5. Laboratory test set-up of the experimental TTU Acoustography system showing its major components, such as work station, optics/electronics housing, immersion tank, and scanner head unit containing the AO sensor, sound source and sample (close-up view).

of [[0/45/0/45]2]S and each measured approximately 300 mm × 300 mm (11.8″ × 11.8″) with a cross-sectional thickness of approximately 3.4 mm (0.13″) as shown in Fig. 4. Similarly, panel C was a step-wedge laminate, with similar ply orientation as A and B but varied from 2 to 28 plies and measured approximately 150 mm × 350 mm (5.9″ × 13.8″), with a cross-sectional thickness ranging from approximately 0.4 mm - 5.9 mm (0.02” - 0.23″).

3.2. Laboratory TTU Acoustography system

The actual laboratory test set-up for the TTU Acoustography system is shown in Fig. 5. The sound source used was fabricated using a 76 mm × 76 mm (3″ × 3″) Piezo-electric plate with a center frequency of 5 MHz. The AO sensor used was selected to have an operating frequency of 5 MHz, to match that of the sound source.

3.3. Conventional immersion TTU C-scan system

The laboratory conventional immersion TTU C-scan system with associated instrumentation is shown in Fig. 6. Tests were conducted at 5 MHz by utilizing a pair of flat transducers with an element size of 9.5 mm (0.375″). During the immersion TTU scans test panels were placed in the far-field of the transducers, at a distance approximately 76 mm (3″). A 125 MHz sampling rate was used, with scan indexing increments of 1 mm (0.004″) and a scan speed of 5.1 mm/s (0.2 inch/sec).

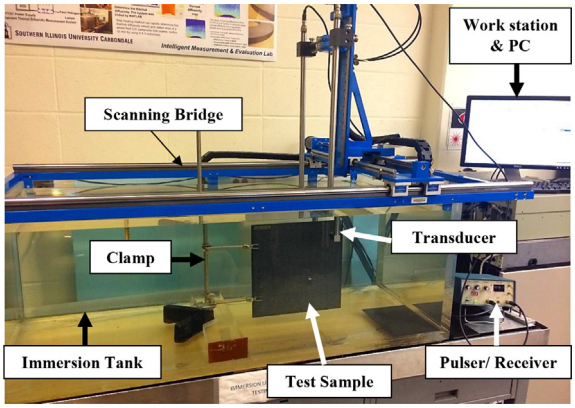

Fig. 6. Laboratory test set-up of the conventional immersion TTU C-scan system, showing the major components such as the work station, immersion tank, scanning bridge, transducer, and sample.

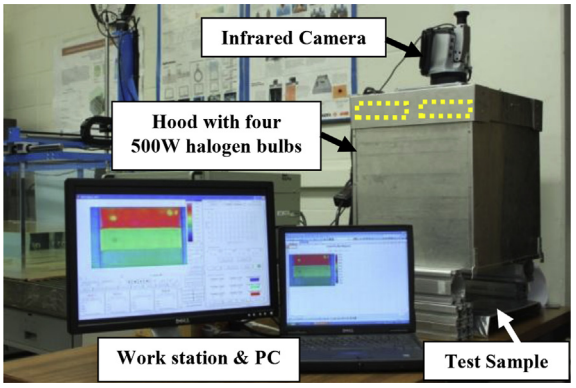

Fig. 7. Laboratory test set-up of the infrared thermography system, showing the major components such as the work station, infrared camera, hood, and sample. The micro-controller for controlling the heat source is hidden behind the laptop and is not shown in the figure.

3.4. Infrared thermography system

The experimental setup used for conducting infrared thermography tests is shown in Fig. 7. This is a custom-made laboratory infrared thermography system which is similar to that described in an outside work [1,34]. During experimentation, a continuous and uniform heat flux was applied for approximately 5 s. The sample was then allowed to cool, and the temperature responses were recorded, which allowed for a temperature variation within the discontinuous areas. The infrared camera recorded the data between the time interval from approximately 3 s prior to heating and up to 12 s after heat was removed.

4. Results

The experimental results obtained from each of the composite test panels by using the three different NDE techniques is presented, including their quantitative comparisons.

4.1. TTU Acoustography

The raw (unprocessed images) TTU Acoustography results for the three CFRP test panels containing various simulated FOI defects are shown in Fig. 8. Prior to testing, the AO sensor was calibrated to relate AO sensor brightness to ultrasound power. This was obtained by measuring the brightness as a function of ultrasound power without the test part and then with the test part, respectively. The 255 gray scale shades in the images shown represents the ultrasound attenuation variation across the sample; darkest shade (i.e. 0) representing the highest attenuation and brightest shade (i.e. 255) representing the lowest attenuation. FOIs in the test panels exhibited higher acoustical impedance than the CFRP, which attenuated the transmitted ultrasonic signals. All images were acquired in near real-time. In order to generate full size panel scans, proprietary Acoustography software was used. A series of images were recorded in sequence and stitched together creating an acoustic mosaic image of the panel.

4.2. Conventional immersion TTU C-scan

Conventional immersion TTU testing was conducted for direct comparison and validation of TTU Acoustography on all test panels. 5 MHz immersion TTU C-scan results for composite panels are shown in Fig. 9. The 255 gray scale shades in the images shown represents the ultrasound attenuation variation across the sample;

darkest shade (i.e. 0) representing the highest attenuation and brightest shade (i.e. 255) representing the lowest attenuation. Likewise Acoustography results, FOIs in the test panels exhibited higher acoustical impedance than the CFRP, which attenuated the transmitted ultrasonic signals as shown in immersion TTU C-scan results.

4.3. Infrared thermography

Infrared thermography (IRT) test results obtained for all test panels are shown in Fig. 10. The IRT results shown are the best thermal image response in the sequence, having the highest thermal contrast, was captured around 8.5 s (i.e., during the initial cooling stage). FOIs in the test panels exhibited higher thermal contrast and appeared as "hot spots" in the IRT image results. The highest thermal contrast images were used for further analysis.

5. Discussions

From the results presented in Figs. 8–10, it is demonstrated that the ability of TTU Acoustography to detect all FOI defects in graphite epoxy composite laminates is in strong correlation with

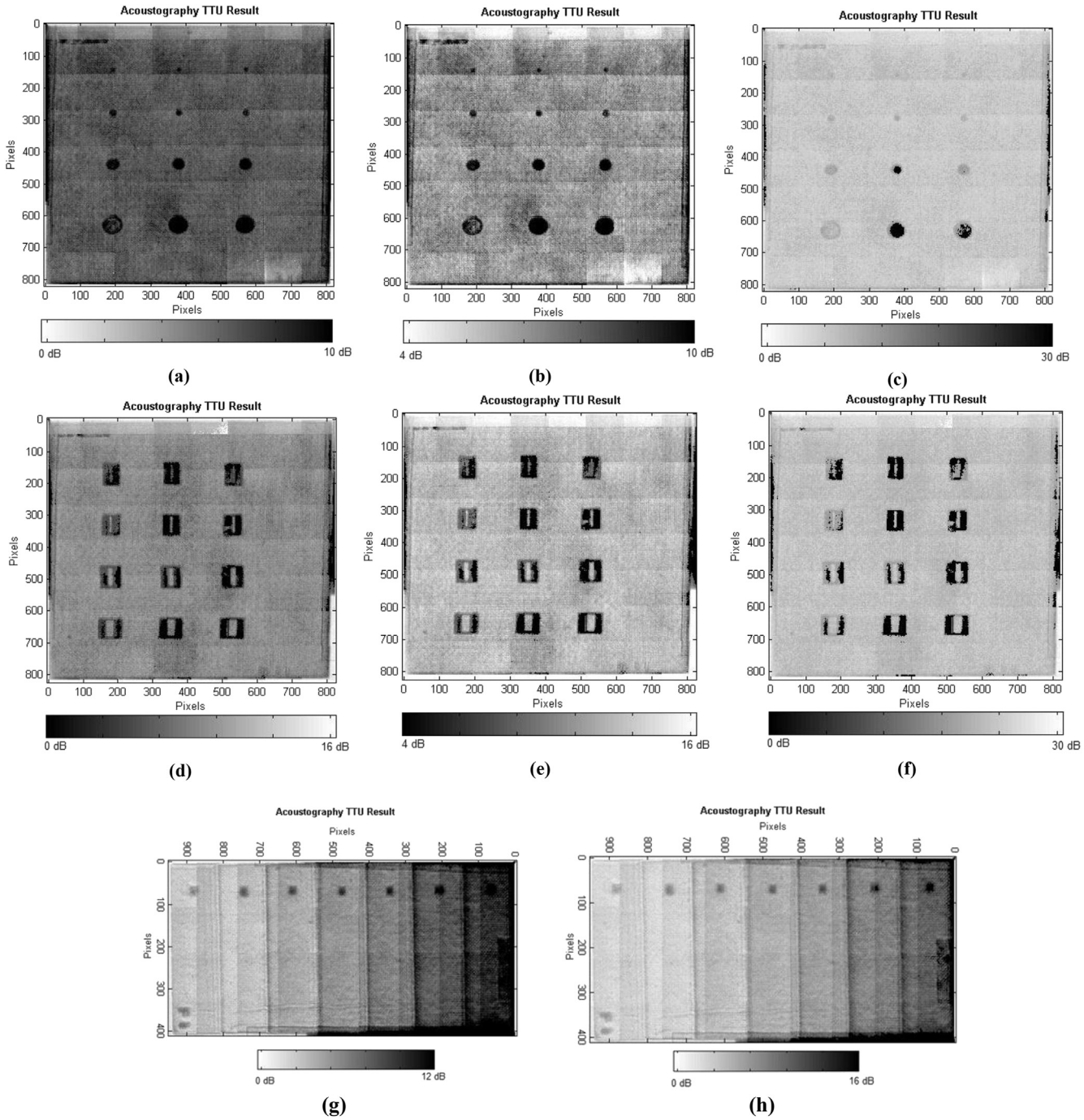

Fig. 8. 5 MHz TTU Acoustography results for CFRP panels with embedded FOI defects. (a)–(c) Panel A at 0–10 dB, 4–10 dB, and 0–30 dB; (d)–(f) Panel B at 0–16 dB, 4–16 dB, and 0–30 dB; and, (g)–(h) Panel C at 0–12 dB, and 0–16 dB respectively.

conventional immersion TTU and IRT techniques. It is also demonstrated that the Acoustography technique was able to detect the smallest inclusion, having a diameter of 3 mm (0.12″), embedded at different layers as shown in Fig. 8(a–c). In addition, this novel technique was also able to more clearly resolve FOI defects embedded at different layers separated by only a 1.5 mm (0.06″) gap distance as shown in Fig. 8(d–f). Furthermore, the fibrous nature of the composite panels was also more evident in the Acoustography imaging results. The Acoustography method seemed to exhibit a higher definition/resolution of the defects as compared to our immersion TTU C-scans and IRT results shown in Figs. 9 and 10. The superior definition of defects and the fibrous nature of the specimen may be attributed to the superior pixel resolution of the AO-sensor used in this novel technique: sensing LC molecules in the AO-sensor are in the order of 20 Å. Although, the AO-sensor pixel resolution is very fine, the pixel resolution of the camera and monitor is much lower compared to that offered by the AO-sensor. Accounting for the lower resolution of the camera, monitor and the magnification factor, the effective pixel resolution of the Acoustographic images was determined to be 0.2 mm (0.008″).

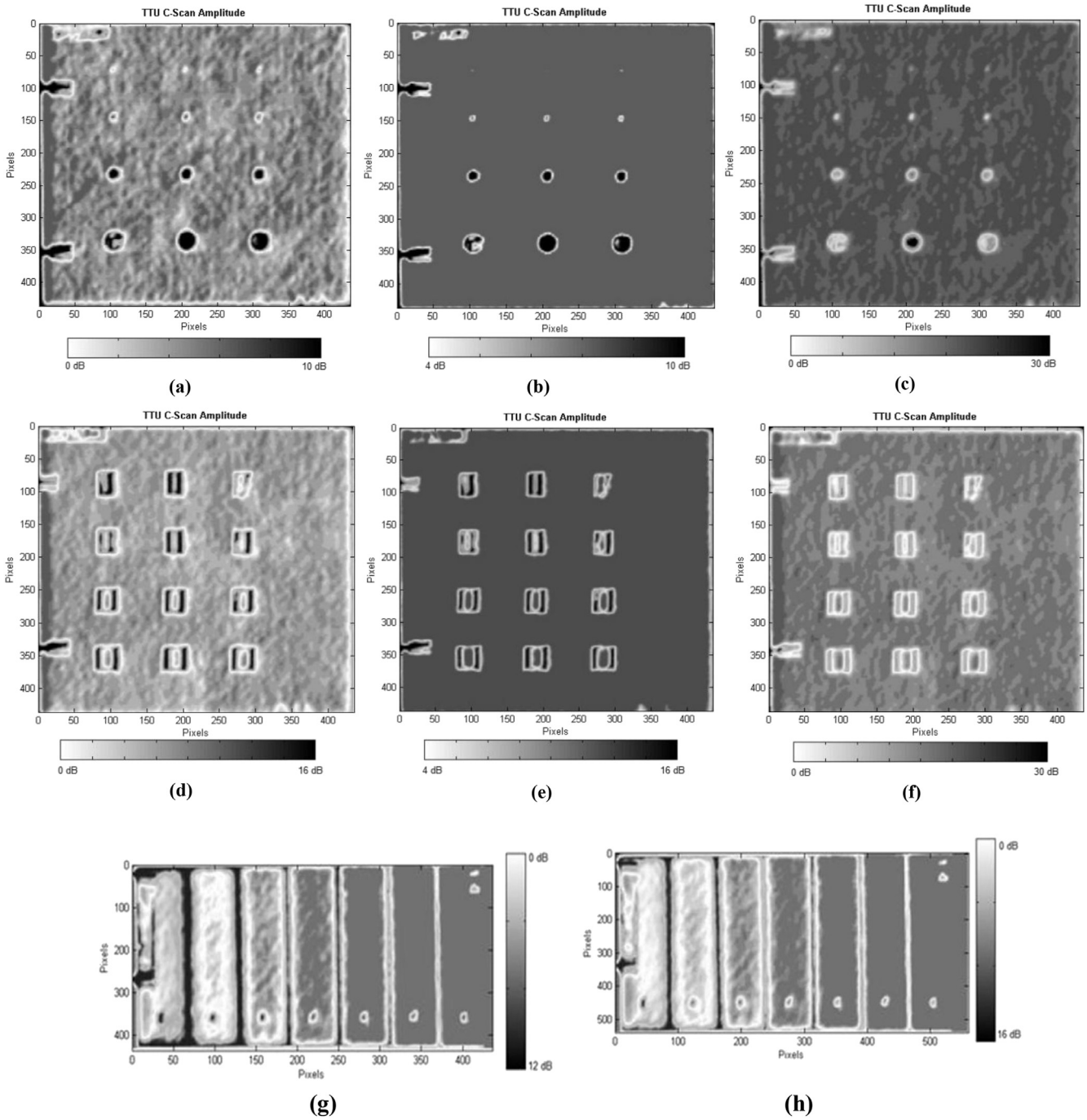

Fig. 9. Conventional immersion TTU results for CFRP panels with embedded FOI defects at 5 MHz (a)–(c) Panel A at 0–10 dB, 4–10 dB, and 0–30 dB; (d)–(f) Panel B at 0–16 dB, 4–16 dB, and 0–30 dB; and, (g)–(h) Panel C at 0–12 dB, and 0–16 dB.

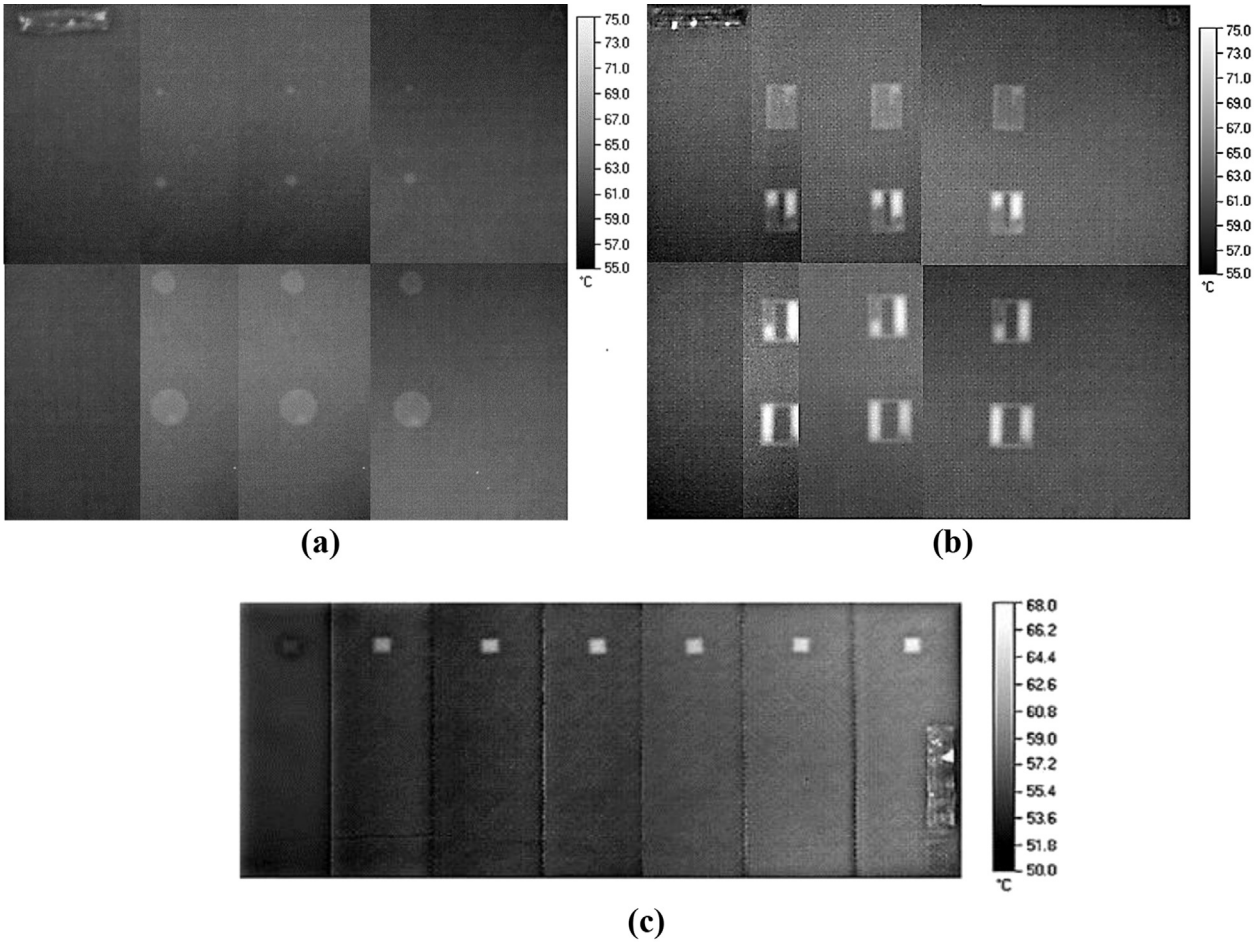

Fig. 10. IRT image results for CFRP panels with embedded FOI defects. (a) Panel A; (b) Panel B; and, (c) Panel C.

5.1. Quantitative comparisons

For quantitative comparisons of results obtained by the three different NDE techniques, Acoustography was directly compared with conventional immersion TTU C-scans and IRT images on the basis of the Signal-to-Noise Ratio (SNR), FOI defect sizing, and inspection times.

The SNR was calculated by using the following formula:

$$SNR = \left(\frac{\mu_{sound} - \mu_{defect}}{\sigma_{sound}} \right) \quad (1)$$

where, μ_{sound} is the mean gray scale value for the sound region, μ_{defect} is the mean gray scale value for the defect region, and σ_{sound} is the standard deviation value of gray scale for the sound region. The histograms shown in Fig. 11, are the mean and standard deviation values for the sound and defect regions in panel A for all three NDE techniques utilized. These were used to calculate SNR for each different NDE technique that was applied for this research work.

Table 1 compares the SNR for the three NDE methods, Acoustography, conventional immersion TTU C-scan, and IRT for the three different CFRP panels with embedded FOI defects. From the results presented, SNR measurements for Acoustography were more than 6:1 and are also in good correlation with conventional immersion TTU and IRT results.

Similarly, defect sizing measurements were conducted in panel A, row 1 FOI defects, for each of the NDE techniques. Defect sizing was calculated by first calibrating the image scale to its original dimension and then by applying Sobel edge detection algorithm in ImageJ. Fig. 12 shows the processed image results for panel A and the line profile plots across row 1 FOI defects (represented by the red line superimposed on the images) for each of the NDE methods.

Table 2 lists the FOI defect sizing measurements for panel A, row 1 FOI defects for each of the NDE techniques applied. From the results presented in Table 2, it is demonstrated that the defect sizing ability of TTU Acoustography for FOI defects in graphite epoxy composite laminates is in strong correlation with the both conventional immersion TTU and IRT techniques.

Lastly, the inspection times for each of the NDE methods applied for this research were compared. Table 3 shows the inspection time results for a 300 mm × 300 mm (11.8″ × 11.8″) panel. The inspection time required using TTU Acoustography was about three minutes and was much faster compared to IRT (10 min) and conventional immersion TTU techniques (three hours). Table 3 compares typical inspection times for the three NDE methods to scan a 300 × 300 mm (11.8″ × 11.8″) composite panel.

It is to be noted that the TTU C-scan inspection time was relatively higher because tests were conducted by using an older immersion UT system. Current modern state-of-the-art gantry/squirter TTU UT systems, now provide higher scanning speeds in the X–Y axis, that can achieve 300 mm/s (11.8 in/s) and with a 0.5 mm (0.02″) indexing, and requiring 600 passes to scan a 300 mm × 300 mm (11.8″ × 11.8″) composite panel, can thus reduce its inspection time to approximately 10 min, rivaling IRT

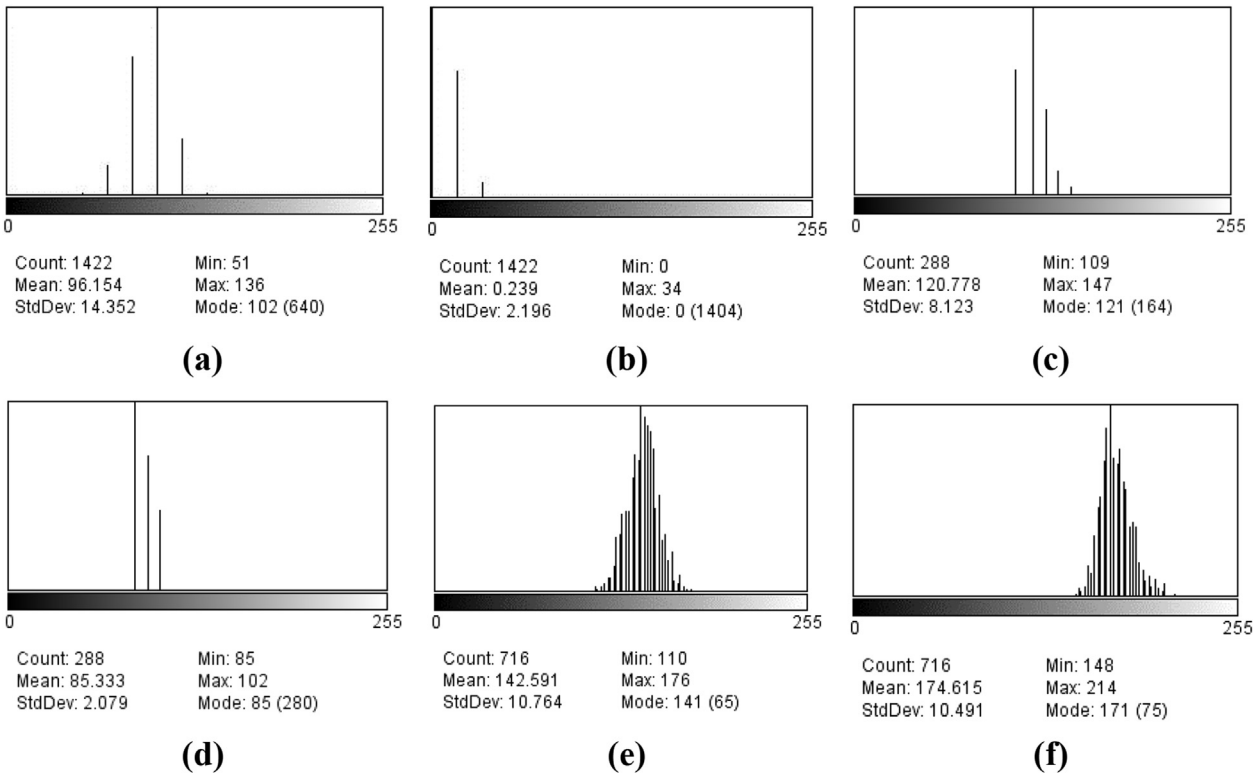

Fig. 11. Histograms showing mean and standard deviation values for the sound and defect regions in panel A. (a) Sound region-Acoustography 0–10 dB result; (b) Defect region-Acoustography 0–10 dB result; (c) Sound region-immersion TTU 0–10 dB result; (d) Defect region-immersion TTU 0–10 dB result; (e) Sound region-IRT result; and (f) Defect region-IRT result.

Table 1
Signal-to-Noise Ratio (SNR) measurements.

	TTU Acoustography	Immersion TTU C-Scan	IRT
Panel A	6.68	4.36	2.74
Panel B	11.35	4.54	10.18
Panel C	6.39	0.81	7.97

inspection speeds. It should also be mentioned that Acoustography scan times can be dramatically reduced by using even larger field of view (FOV) Acoustography NDE systems. For example, currently, a prototype 30.5 mm × 30.5 mm (12″ × 12″) full FOV Acoustography NDE system is under development. Thus, this system will be able to inspect the full field in only 10 s, providing 60 times the speed advantage over traditional point-by-point TTU scans.

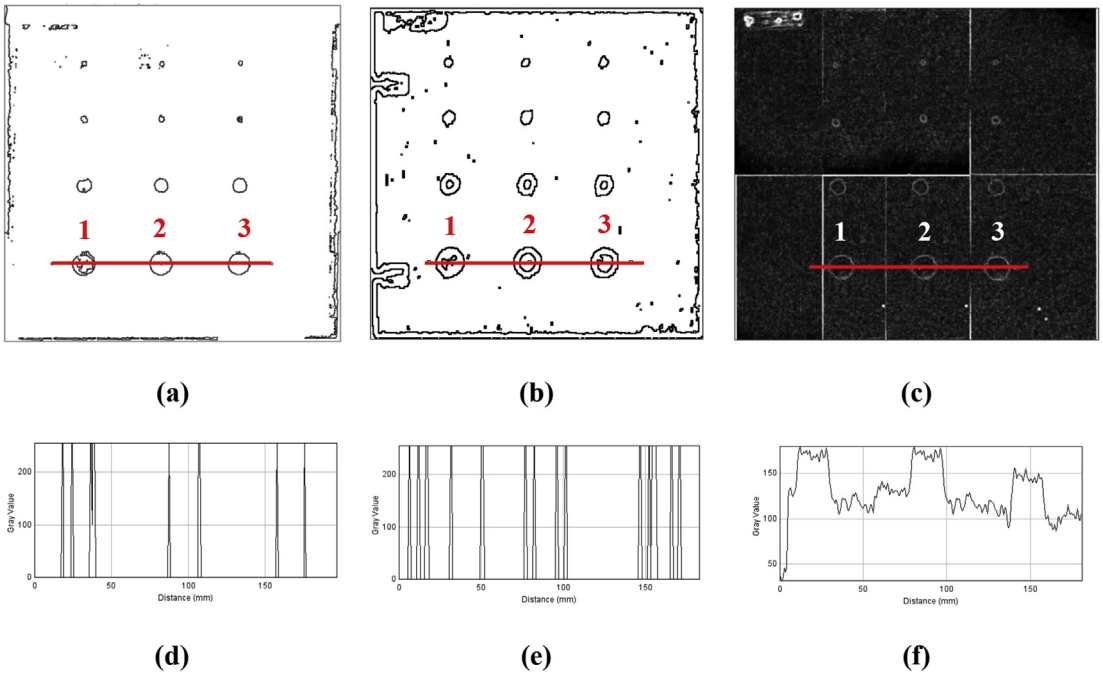

Fig. 12. Processed image results and line profile plots across row 1 FOI defects of Panel A for defect sizing measurement. (a & d) TTU Acoustography; (b & e) immersion TTU; and, (c & f) IRT.

Table 2
Defect sizing measurements for panel A row 1 FOI defects.

FOI defect#	NDE techniques	Measured diameter (mm)	Actual diameter (mm)
1	TTU Acoustography	19.6	20
	TTU C-scan	19.3	20
	IRT	19.4	20
2	TTU Acoustography	19.2	20
	TTU C-scan	19.3	20
	IRT	19.9	20
3	TTU Acoustography	19.6	20
	TTU C-scan	18.8	20
	IRT	19.4	20

Table 3
Inspection time for three NDE methods utilized.

	Laboratory TTU Acoustography	Conventional immersion TTU C-Scan	IRT
Scan speed	76 mm × 76 mm/shot	5.1 mm/s	100 mm × 150 mm/shot
Indexing steps	76 mm	1 mm	100 mm
Image generation time	10 s	N/A	1 s
Image capture time	30 ms	N/A	18 s
Image storage time	1 s	N/A	20 s
Number of shots	56	N/A	6
Time between shots	1 s	N/A	60sec
Typical inspection time	3 min	3 h.	10 min

Area = 300 mm × 300 mm (11.8″ × 11.8″); Panel Thickness = 3.4 mm (0.132″) (Typical).

6. Conclusion

The TTU Acoustography NDE method was employed to detect FOI defects embedded in carbon fiber epoxy composite laminates. Three different composite test panels with varied size FOI defects embedded at varying depths were considered for this work. The Acoustography method, operating at 5 MHz, and was easily able to detect FOI defects in the test composite laminates. A side-by-side comparison of Acoustography technique with convention immersion TTU and IRT techniques showed very good correlation between the three NDE methods in detecting FOI defects within the composite test panels. The lateral resolution of TTU Acoustography was found to be superior to the conventional TTU C-Scan method. Also, the flaw detection sensitivities of Acoustography were also found in very good agreement to the conventional TTU C-Scan and IRT methods.

Finally, from the operator's point of view, the Acoustography technique was shown to be significantly simpler to operate and results determined and defined do to the minimal skill level required for its inspection process. Currently, a prototype 30.5 mm × 30.5 mm (12″ × 12″) full FOV Acoustography NDE system is undergoing development and testing. This will further reduce the number of images required to inspect larger parts, thereby proving a, an even more dramatic increase in inspection speed compared to other existing techniques.

References

[1] Chu TP, Poudel A, Filip P. C/C composite brake disk non-destructive evaluation by IR thermography. In: SPIE thermosense – thermal infrared applications XXXIV; 2012. p. 8354.
[2] Chu TP, Don J, Pan Y, Poudel A. Defect characterization in commercial Carbon-Carbon composites. World J Eng 2012;9(6):481–6.
[3] Poudel A, Chu TP. Intelligent nondestructive testing expert system for aircraft Carbon/Carbon composite brakes using infrared thermography and Air-coupled ultrasound. Mater Eval 2012;70(10):1219–29.
[4] Poudel A, Strycek J, Chu TP. Air-Coupled ultrasonic testing of Carbon/Carbon composite aircraft brake Disks. Mater Eval 2013;71(8):987–94.
[5] Poudel A, Sandhu JS, Chu TP, Pergantis C. Porosity measurement in carbon fiber epoxy laminates by using acoustography. In: ASNT – 23rd annual research symposium and spring conference; 2014 [Minneapolis, MN].
[6] Matzkanin GA, Yolken HT. Techniques for the nondestructive evaluation of polymer matrix composites. AMMTIAC Q 2008;2(4):3–7.
[7] Cawley P, Adams RD. The mechanics of the Coin-Tap method of non-destructive testing. J Sound Vib 1988;122(2):299–316.
[8] Djordjevic BB. Advanced ultrasonic probes for scanning of large structures. In: Proc – ultrasonic international. Vienna, Austria: Butterworth Heinemann; 1993.
[9] Hsu DK, Hughes MS, Patton TC. Ultrasonic scans using low-frequency unresolved echos. Rev Prog Quantitative Nondestruct Eval 1993;12:1595–602.
[10] Kommareddy V, Peters JJ, Hsu DK. Air-coupled ultrasonic measurement in composites. In: Proc. SPIE: 3rd Intl. Conference on experimental Mechanics, 5852; 2004. p. 105–11.
[11] Cerniglia D, Montinaro N, Nigrelli V. Detection of disbonds in multi-layer structures by laser-based ultrasonic technique. J Adhesion 2008;84(10):811–29.
[12] Poudel A, Strycek J, Chu TP. Air-coupled ultrasonic testing of carbon-carbon composite aircraft brake disks. Mater Eval 2013;71(8):987–94.
[13] Li S, Poudel A, Chu TP. Ultrasonic defect mapping using signal correlation for NDE. RNDE 2014;26(3). http://dx.doi.org/10.1080/09349847.2014.967900.
[14] Vavilov V, Kourtenkov D, Grinzato E, Bison P, Marinetti S, Balageas D. Thermal characterization of defects in carbon fibre reinforced plastics: comparison of some inversion procedures. In: Proc – International symposium on nondestructive testing in civil engineering, 1; 1995. p. 551–8.
[15] Cramer KE, Winfree WP. Thermal characterization of defects in aircraft structures via spatially controlled heat application. In: Proc. International conference on thermal sensing and imaging diagnostic applications – thermosense XVIII; 1996. p. 202–9.
[16] Maldague X, Marinetti S. Pulse phase infrared thermography. J Appl Phys 1996;79(5):2694–8.
[17] Maldague X. Theory and practice of infrared technology for nondestructive testing. Newyork: Wiley; 2001.
[18] Rajic N. Principal component thermography for flaw contrast enhancement and flaw depth characterisation in composite structures. Compos Struct 2002;58(4):521–8.
[19] Shepard SM, Lhota JR, Rubadeux BA, Wang D, Ahmed T. Reconstruction and enhancement of active thermographic image sequences. Opt Eng 2003;42(5):1337–42.
[20] Newman JW, Lindberg J. Laser shearography of wind turbine blades. Mater Eval 2010;68(7):828–37.
[21] Chu TP. NDE of RCC using digitome volumetric x-ray imaging system. In: Proc. SEM annual conference & exposition on experimental and applied mechanics; 2006 [St. Louis, MO.].
[22] Shedlock D, Edwards T, Toh C. X-Ray backscatter imaging for aerospace application. In: Proc. 37th annual review of progress in quantitative nondestructive evaluation (QNDE); 2011. p. 509–16.
[23] Liu CTB, Huang MJ, Pan YP, Shedlock D, Chu TP. Detection of discontinuities in carbon-carbon composites using x-ray Compton backscatter radiography: radiography by selective detection. Mater Eval 2012;70(3):367–77.
[24] Schilling PJ, Karedla BPR, Tatiparthi AK, Verges MA, Herrington PD. X-ray computed microtomography of internal damage in fiber reinforced polymer matrix composites. Compos Sci Technol 2005;65(14):2071–8.
[25] Qaddoumi N, Carriveau G, Ganchev S, Zoughi R. Microwave imaging of thick composites with defects. Mater Eval 1995;53(8):926–9.
[26] Sandhu JS, Wang HH, Popek WJ. Acoustography for rapid ultrasonic inspection of composites. In: SPIE – nondestructive evaluation of materials and composites, 2944; 1996. p. 117–24.
[27] Sandhu JS, Wang HH, Popek WJ, Sincebaugh P. Acoustography: a side-by-side comparison with conventional ultrasonic scanning. In: SPIE – nondestructive evaluation of aging materials and composites, 3585; 1999. p. 163–72.
[28] Sandhu JS, Wang HH, Popek W, Sincebaugh PJ. Acoustography: It could be a practical ultrasonic NDE tool for composites. In: SPIE – nondestructive evaluation of materials and composites V, 4336; 2001. p. 129–34.
[29] Sandhu JS, Wang HH, Sonpatki MM, Popek WJ. Real-time full-field ultrasonic inspection of composites using acoustography. In: SPIE – nondestructive evaluation and health monitoring of aerospace materials and composites, 5046; 2003. p. 99–104.
[30] Sandhu JS. Non-Coherent frequency source and sector scanning apparatus for ultrasonic imaging system using a liquid crystal detector cell. U. S. P. Office; 1987.
[31] Sandhu JS, Thomas RE. Acoustographic nondestructive evaluation. In: IEEE – ultrasonics symposium, 1052; 1988. p. 1053–6.
[32] Sandhu JS. Acoustography: a new imaging technique and its applications to nondestructive evaluation. Mater Eval 1988;46(5):608–12.
[33] Sandhu JS. Nondestructive testing handbook. ASNT; 1995.
[34] Poudel A, Kanneganti R, Gupta L, Chu TP. Nearest mean classifier for defect classification in CFRP panels. In: ASNT - 22nd research Symposium and Spring Conference; 2013 [Memphis, TN.].